Article

The International Journal of Robotics Research
2015, Vol. 34(1) 26–42

DOI: 10.1177/0278364914555544
ijr.sagepub.com
SAGE

Robot grasp planning based on demonstrated grasp strategies

Yun Lin and Yu Sun

Abstract

This paper presents a novel robot grasping planning approach that extracts grasp strategies (grasp type, and thumb placement and direction) from human demonstration and integrates them into the grasp planning procedure to generate a feasible grasp concerning the target object geometry and manipulation task. Our study results show that the grasp strategies of grasp type and thumb placement not only represent important human grasp intentions, but also provide meaningful constraints on hand posture and wrist position, which highly reduce both the feasible workspace of a robotic hand and the search space of the grasp planning. This approach has been thoroughly evaluated both in simulation and with a real robotic system for multiple daily living representative objects. We have also demonstrated the robustness of our approach in the experiment with different levels of perception uncertainties.

Keywords

Grasp planning, human demonstration, grasp type, thumb placement

1. Introduction

There is general agreement that the crucial feature distinguishing the human hand from other apes' hands is the opposable thumb (Napier, 1960, 1965; Susman, 1998; Marzke and Marzke, 2000; Young, 2003). The long, strong and mobile opposable thumb, combined with the other shortened fingers, make possible sophisticated manipulative skills and tool-using, whereas the hands of apes, who are considered to be closest to humans, are evolved mainly for climbing but not for manual dexterity. Without an opposable thumb, humans would not be able to develop efficient grasping and dexterous manipulation skills.

In Napier (1965), the opposable thumb characterizes humans by two basic grasp types for all prehensile activities: the precision grip, in which objects are gripped by only fingertip of the thumb and some fingers, and the power grip, in which objects are wrapped around by thumb and some fingers. Derived from these two basic grips, Cutkosky (1989) developed a hierarchical tree of grasp types to facilitate the design and control of robotic hands for various manipulation purposes. Almost all grasp types in the taxonomy, even as simple as a two-finger precision grip, are formed by thumb and some other fingers. The grasp types defined in other alternative grasp taxonomies (e.g. Dai et al., 2013) also have similar features. The only exception is the non-prehensile grasp, which does not require the thumb at all. Similarly in robotics Oztop and Arbib (2002) simplified the robotic models to a thumb and virtual finger (defined by a set of fingers opposing a thumb). Such robotic hand models include all the popular hand models such as the NASA Robonaut hand (Lovchik and Diftler, 1999), the Shadow hand (Kochan, 2005), the Utah/MIT hand (Jacobsen et al., 1984) and the DLR Hand II (Butterfass et al., 2001), PR2 gripper, etc. To meet a specific task requirement and object shape, the robotic hand can choose one particular grasp type from the taxonomy. Once the thumb is placed on the target object, the other fingers can be placed naturally against the thumb to form that particular grasp. Clearly, thumb and grasp types are closely related, and they are two critical features that characterize a human grasp.

In this paper, we propose a novel grasp synthesis approach that integrates two human grasp strategies – grasp type, and thumb placement (position and direction) – into grasp planning. The proposed technique fits in the learning from demonstration (LfD) framework that allows robots to learn skills from humans. One application of LfD is to

Department of Computer Science and Engineering, University of South Florida, FL, USA

Corresponding author:
Yu Sun, Department of Computer Science and Engineering, University of South Florida, 4202 E Fowler Avenue, ENB 118, Tampa FL, 33620, USA.
Email: yusun@cse.usf.edu

abstract human grasping strategies from demonstration such that the skill abstraction can meet two important criteria: it should reflect the demonstrator's intention, and it should be general enough to be used by a robotic hand distinct from human. Different abstractions of human grasp constrain the grasp synthesis and narrow down the solutions of grasp generation to different levels. If imposing a strict constraint, such as defining all contact points of the fingers on the object, it loses flexibility and becomes rarely achievable for a robotic hand with a different kinematic model. Thus, the choice of grasp strategies should balance the learned constraints and required flexibility to accommodate the difference between the human and robotic hands. The human strategies of grasp type and thumb have such a balance while conveying important human intentions to the robotic grasping.

Grasp types abstract the manner in which a human grips an object for a manipulation. One example is the procedure of screwing on a jar lid, which starts with a precision grasp using only the fingertips, because the jar lid is loose at the beginning and can be screwed efficiently and flexibly without much power. As the jar lid gets tighter, one may switch to a power grasp to apply larger force to the jar lid.

Nevertheless, grasp type cannot by itself form appropriate contact points on the object. It has to be combined with the suitable grasp region and direction. Thus, we learn thumb placement and direction as the second grasp cue from humans, mainly for two reasons discussed above. Firstly, almost all robotic hands have a long and strong opposable thumb, although robotic hands are usually simplified to different extents from the human hand, so thumb placement and direction is also independent of robot kinematics. Secondly, the thumb plays a key role in gripping an object efficiently, according to the anthropology research. In some sense, thumb placement indicates which surface or part of the object to be gripped. It also constrains the workspace of the wrist and other fingers while preserving the necessary flexibility to meet kinematic constraints.

The grasp type and thumb placement establish a grasp strategy that confines the configuration space of the wrist as well as the hand, but they cannot fully determine a grasp or guarantee that a grasp is stable. The confined space leaves enough room for grasp planning to find the optimal stable grasp that is adapted to different robotic hand models.

In this paper, we provide a detailed discussion on how the proposed grasp strategies can be obtained and how they are beneficial for establishing a robotic grasp. Grasp type can be input by the human or recognized from human demonstration. A novel recognition approach using trajectory data at joint level is presented in Section 3. Thumb information can also be observed from human demonstration, or labeled directly on the object surface, as discussed in Section 4. We believe that grasp type and the thumb are simple, effective and informative representations of the grasp features.

2. Related work

Numerous works have been done to abstract various useful grasp features from human grasp. Grasp features can be learned by observing human demonstration. Perhaps the most straightforward way of learning from human demonstration is direct mapping, either in joint space (Fischer et al., 1998) or fingertip workspace (Peer et al., 2008). Mapping in joint space is suitable for power grasps but not for precision grasps. Mapping in fingertip space, on the other hand, is more suitable for precision grasps. Direct mapping imposes a strict constraint on the robot grasp, leading to the lack of flexibility that is required to compensate for the kinematics/geometry difference between the robotic and human hands. Recently, estimating the demonstrator's hand posture from vision (Hueser et al., 2006) became possible and accessible and led to promising work that transferred the hand posture to robotic hands with dissimilar kinematics (Gioioso et al., 2011). The methods presented in Li et al. (2007), Papazov et al. (2012) and Kootstra et al. (2012) are similar, where shape or object feature matching algorithms were applied to match hand poses from similar objects in a database. Instead of direct mapping, grasp types can be recognized and mapped to different robotic hands (Ekvall and Kragic, 2005; Aleotti and Caselli, 2006; Heumer et al., 2007). However, the grasp type alone cannot form good grasps. Therefore, some researchers introduced additional information to grasp type. Kang and Ikeuchi (1997), Zöllner et al. (2005), Tegin et al. (2009) and Romero et al. (2009) abstracted an approach vector together with grasp type to map the location and pose of the robot hand from human demonstration. The approach vector can only be obtained by observing human demonstration. It provides a good initial pose to start with, but it does not indicate which surface or part of the object to be gripped.

Alternatively, grasp features can be abstracted based on the observation of the object (Sahbani et al., 2012). One approach is to learn contact points on an object's surface (Nguyen, 1988; Ponce and Faverjon, 1995; Zhu and Wang, 2003; Liu et al., 2004; Roa and Suárez, 2009; Le et al., 2010), which has the problem of solving the inverse kinematics that satisfy the constraints imposed by contact points (Rosales et al., 2011) and does not work well for power grasps. Pollard (2004) presented an efficient data-driven algorithm for grasp synthesis by providing successful grasp examples. Contact regions are projected to the object surface by preserving similar quality measures from a demonstrated grasp. In Saxena et al. (2008), a database was collected by labeling grasp points on 2D images on the object. Kim (2007) adapted the contact point approach to similar objects by finding point-to-point correspondence between two meshes. The approach proposed in Ben Amor et al. (2012) learned grasp types from demonstration and generalized contact points by the contact warping algorithm, but since contact points were learned to generate the grasp, no power grasps were being tested on the robot.

Similar work was presented in Hsiao and Lozano-Perez (2006), who used hand shape sequence and contact locations as human grasp features.

Transferring grasp features to a robot may generate unstable grasp candidates. Thus, numerous works, such as Kim (2007), Gioioso et al. (2011) and El-Khoury and Sahbani (2010), combined grasp quality analysis with human grasp strategies to find force-closure grasps close to human demonstration.

3. Grasp taxonomy and classification

The grasp type can either be input by the human teacher, or recognized from the human demonstration. In this section, a novel grasp recognition approach using grasp motion trajectories at joint level is presented.

Many grasp classifications are defined based on Cutkosky's grasp taxonomy (Cutkosky, 1989), which classifies user-performed grasps into 16 classes that vary by task requirement and dexterity. To recognize the demonstrated grasp as a type from Cutkosky's taxonomy, pattern classification techniques can be applied.

Ekvall and Kragic (2005) used hidden Markov models to recognize grasp type from the taxonomy based on an entire grasp sequence. The recognition rate was 97% for a single user and known objects existing in both the training and test dataset when there are 10 grasp types. The recognition rate dropped to 65% for known objects and unknown users that were not in the training dataset. There is no information on performance when unknown objects were tested. Aleotti and Caselli (2006) performed grasp recognition using static grasp poses in virtual reality for six grasp types, with a recognition rate of 94% for two expert users without using real objects. Heumer et al. (2007) compared the different classification methods for recognizing six grasp types. The best recognition rate of all the methods was 83.82% for known users and 71.67% for both unknown users and objects.

Our previous work (Lin et al., 2012; Lin and Sun, 2013a) has shown that trajectories of the hand joints provide more information than static poses. It is necessary to disambiguate between different grasp types that share similar static poses but differ in grasp trajectories, because some similar poses belonging to different classes in the human hand configuration space may be far apart from each other in the robotic hand configuration space. For example, the lateral pinch and small wrap have similar measures on joint angles using a data glove, whereas, due to much less dexterity in some robotic hands, for example, a Barrett hand, the lateral pinch has to be performed in a way that is distinguishable from the small wrap (Figure 1).

Given a training dataset of grasp motion sequences, the high-dimensional hand motions in the dataset usually have undesirable properties that bias the learning results. Dimensionality reduction is a typical approach for finding a lower intrinsic dimensionality of data while removing the undesirable noise and variance and leaving a minimum number of needed properties of the data. Typical methods for dimensionality reduction include linear methods, such as principal component analysis (PCA) (Hotelling, 1933) and linear discriminant analysis (LDA) (Fisher, 1936), both of which find a linear transformation of high-dimensional data to its low-dimensional counterpart. Nonlinear methods, such as isometric feature mapping (Isomap) (Tenenbaum, 1998), local linear embedding (LLE) (Roweis and Saul, 2000), and Laplacian eigenmap (LE) (Belkin and Niyogi, 2001), can model the manifold of the data in the high-dimensional space. These nonlinear methods do not provide a nonlinear transformation that projects new data points to the latent low-dimensional space.

Fig. 1. Corresponding small wrap and lateral pinch of robotic hand to human hand. They look similar to a human grasp but are different for a robotic grasp. Left: Small wrap grasps for a human hand (top) and a robotic hand (bottom). Right: Lateral pinch grasps for a human hand (top) and a robotic hand (bottom).

For dimensionality reduction, we use locality preserving projections (LPP) (He and Niyogi, 2003) to find the low-dimensional manifold of the training motion data. LPP is a linear technique that combines the benefits of both linear and nonlinear methods (He and Niyogi, 2003). It finds a linear mapping function that minimizes the cost function of LEs; thus, new demonstrated data can be easily projected to the low-dimensional space by a linear transformation computed by LPP. Then, grasp recognition is performed in low-dimensional subspaces.

In this paper, LPP is performed on the motion sequence of finger joints, which ignores the time component, so the result is invariant to time and speed. Figure 2 shows the 3D visualization of the 14D hand-joint sequence captured by a data glove for 12 different grasp types in Cutkosky's taxonomy. It demonstrates the ability of LPP to preserve the locality of the nonlinear structure. Although there is partial overlapping between two classes (such as the beginning of the motion sequence because the hand is initially open for all grasp types), there are distinguishable variances among different classes of grasp sequences but little in-class variance.

A demonstrated grasp trajectory can be recognized as a grasp type by measuring the similarity between the

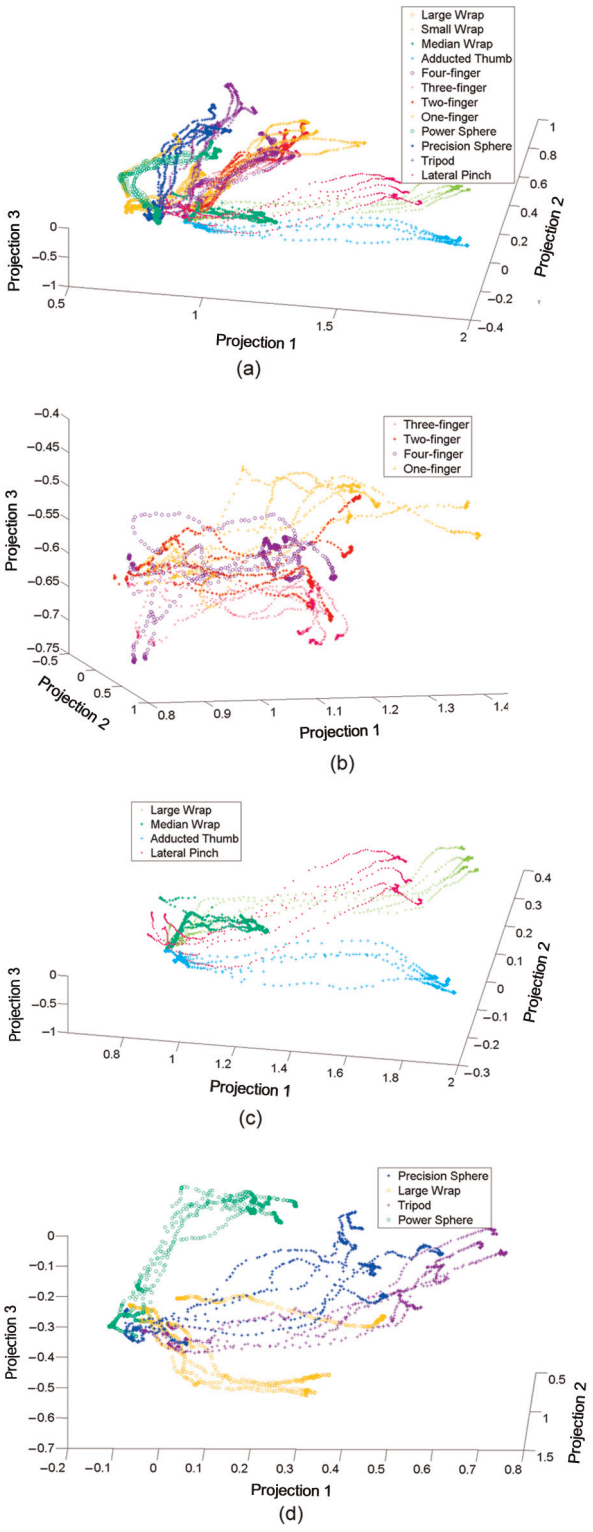

Fig. 2. Three-dimensional visualization of the high-dimensional grasp motion data using LPP; (b)–(d) are subfigures of (a) for better visualization.

demonstrated grasp trajectory and the trajectory in the training dataset. The similarity is defined by Hausdorff distance, described as follows. Let X and Y be two motion trajectories; the Hausdorff distance from X to Y is represented as

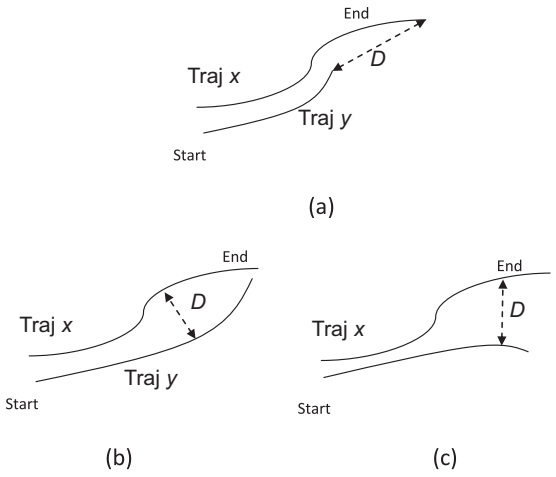

Fig. 3. Three cases of Hausdorff distance between two grasp types. (a) Case 1, trajectory Y is a part of trajectory X; (b) Case 2, trajectories X and Y meet at the end but differ on the way; (c) Case 3, general case, where trajectories X and Y go further away until the end.

$$d_h(X, Y) = \max_{x \in X} \left(\min_{y \in Y} (\| x - y \|) \right) \tag{1}$$

where x and y are data points in trajectories X and Y, respectively. The distance from Y to X is represented as

$$d_h(Y, X) = \max_{y \in Y} \left(\min_{x \in X} (\| x - y \|) \right) \tag{2}$$

The distance between the two trajectories X and Y is defined by

$$D_H(X, Y) = \max(d_h(X, Y), d_h(Y, X)) \tag{3}$$

The Hausdorff distance handles three cases of similarity between grasp motion sequences, as illustrated in Figure 3. The two trajectories start from approximately the same position because they share the same initial pose.

Figure 3(a) demonstrates Case 1, where trajectory Y is roughly a part of trajectory X. This usually happens for the same grasp types but slightly different object sizes. The inter-trajectory distance, therefore, becomes the distance between the end poses of X and Y.

In Case 2 (Figure 3(b)), trajectories X and Y share the same start and end points but differ in intermediate paths. This usually happens when the two grasp types are different but share a similar end pose, such as a lateral pinch and a small wrap, which actually span a larger Euclidean volume in robotic hand configuration space. In this situation, Hausdorff distance is beneficial for distinguishing between two grasp types that share ambiguous grasp poses.

Case 3 (Figure 3(c)) is the general case, in which trajectories X and Y differ in intermediate paths as well as end points.

Hausdorff distance can also be modified to other metrics, such as mean pairwise distance, depending on the applications.

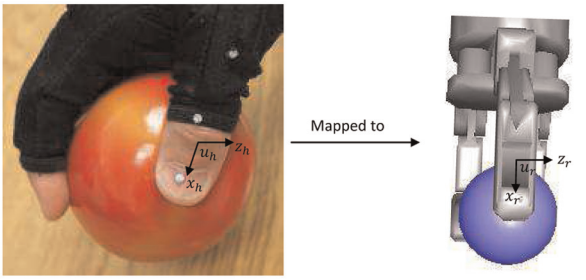

Fig. 4. Translation of thumb placement from human demonstration to the robotic hand.

The *k*-nearest neighbors (*k*NN) method is used to recognize the demonstrated grasp sequence as a grasp type to which the majority of its *k* nearest neighbors belongs.

4. Integration of the extracted strategies into planning

In this section, a Barrett hand model is used as an example to illustrate how the search space of planning is reduced by one thumb position and constrained by grasp types. The thumb position and orientation can be obtained by observing human demonstration or directly labeling on the object.

Grasp planning can be treated as an optimization problem, which searches the maximum value of the high-dimensional quality function Q (e.g. force-closure property). The quality measure is determined by contact points of the hand on the object, and contact points are further determined by the hand posture as well as the relative wrist positions and orientations. Therefore, Q can be a function of hand posture and position:

$$Q = f(p, w) \tag{4}$$

where $p \in R^D$ is the hand posture and $w \in R^6$ is the position and orientation vector of the wrist. The dimensionality D depends on the degrees of freedom (DOFs) of the robotic hand. For a Barrett hand, $D = 4$ and p is a four-joint angle vector:

$$p = \begin{bmatrix} \theta_1 \\ \theta_2 \\ \theta_3 \\ \theta_4 \end{bmatrix} \tag{5}$$

where θ_1, θ_2 and θ_3 are three flexion/extension angles of each finger and θ_4 is one abduction/adduction. Therefore, the quality function Q has 10 variables. An optimal algorithm is needed to search in the high 10D space for the maximum value of the quality function Q. Here, how the search space is reduced to three by teaching relative thumb positions on the object (Figure 4) is discussed as follows.

Figure 5 illustrates the kinematics of a Barrett hand. Define the three fingers of a Barrett hand to be $F1$, $F2$ and $F3$, respectively. Let $\{N\}$ represent a world inertial frame fixed in the workspace. $\{B\}$ is fixed to the object origin. A

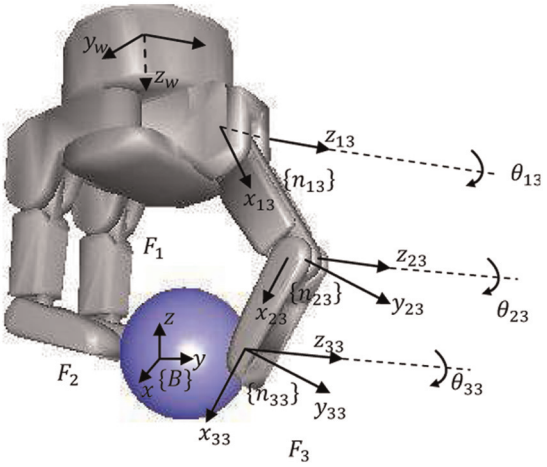

Fig. 5. Barrett hand kinematics. $F1$, $F2$ and $F3$ are the three fingers, with $F3$ being the thumb finger; frame $\{n_w\}$ is attached to the wrist; frame $\{n_{i3}\}$ with axes $\{x_{i3}, y_{i3}, z_{i3}\}$ is attached to each joint of $F3$, where $i = 1,2,3$; θ_{i3} denotes the thumb joint displacement, rotating around rotational axis z_{i3}.

frame $\{n_w\}$ is fixed to the wrist of the robotic hand. Frame $\{n_{ik}\}$ with axes $\{x_{ik}, y_{ik}, z_{ik}\}$ is attached to each joint of the robotic hand, where $i = 1, 2, 3$ is the ith joint of each finger, $i = 3$ represents the end effector, and $k = 1, 2, 3$ is the kth finger. Further, z_{ik} is the rotational axis of joint ik, x_{ik} is the axis along the link ik's principle axis, and y_{ik} is perpendicular to z_{ik} and x_{ik}. Let θ_{ik} denote the joint displacement rotating around rotational axis z_{ik}. Finger $F3$ is usually defined as the thumb, except for one case when lateral pinch is applied (see experiments in Section 5).

Let $u_h \in \Re^6$ denote the vector representing the position and orientation of the center of a human thumb relative to an object coordinate (Figure 4); u_h can be mapped to u_r, the center of the thumb fingertip of the robotic hand, via linear translation. Another way of representing the position and orientation of the robot thumb fingertip with respect to $\{B\}$ is a homogeneous transformation matrix:

$$A_{33} = \begin{bmatrix} R_{33} & d_{33} \\ 0 & 1 \end{bmatrix} \tag{6}$$

where R_{33} is the 3×3 rotation matrix and d_{33} is the three-position vector. If the value of thumb positions and orientations are completely mapped to the robotic hand, contact points of the other fingers on the object may vary tremendously caused by kinematic difference; then, a nonforce-closure grasp may be applied by the robot. Therefore, we exclude θ_{33}, the pitch of the thumb fingertip relative to the object coordinate, from the mapping. Hence, the matrix A_{33} is not constant, but varies as the joint displacement θ_{33} around axis z_{33} adapts to a new value to achieve a force-closure grasp. So, A_{33} is a function of a single joint variable θ_{33}:

$$A_{33} = A_{33}(\theta_{33}) \tag{7}$$

Similarly, A_{i3} is the homogeneous transformation matrix of the ith joint with respect to the frame $\{n_{(i+1)3}\}$. Thus, the homogeneous transformation matrix that expresses the position and orientation of the wrist with respect to the thumb fingertip $n_{(i+1)3}$ is denoted by ${}^{33}T_w$:

$$ {}^{33}T_w = A_{33}(\theta_{33})A_{23}(\theta_{23})A_{13}(\theta_{13})A_w \tag{8} $$

where joint angles θ_{13} and θ_{23} are moved jointly by one motor, and θ_{13} and θ_{23} can be determined by the motor-to-joint transform from motor revolution θ_3:

$$ \begin{bmatrix} \theta_{13} \\ \theta_{23} \end{bmatrix} = \begin{bmatrix} a \\ b \end{bmatrix} \theta_3 \tag{9} $$

The position and orientation of the wrist can be represented as a function of θ_{33} and θ_3 given by the transformation matrix ${}^{33}T_w(\theta_{33}, \theta_3)$. Therefore, the six-position-and-orientation vector w in equation (4) can be determined as a function of θ_{33} and θ_3. Combining equations (4), (5), (8) and (9), equation (4) is expressed as a function of

$$ Q = f(\theta_1, \theta_2, \theta_3, \theta_4, \theta_{33}) \tag{10} $$

where θ_3, θ_4 and θ_{33} determine the position and orientation of the wrist, thumb flexion/extension, and hand adduction/abduction. The flexion/extension of the other two fingers, θ_1 and θ_2, can be determined easily by a simple execution of a close command, so that θ_1 and θ_2 are commanded to conform to the surface of the object. Hence, equation (10) can be simplified as

$$ Q = f(\theta_3, \theta_4, \theta_{33}) \tag{11} $$

Mapping only thumb position from a human hand to a robot hand is simple because there is little correspondence problem and it can be easily generalized to different robotic hand models. By learning partial hand information from the demonstration, we know a reference contact position on the object, and the search space for optimization during the planning procedure is reduced to three. Figure 6 compares the 2D workspace of the wrist with and without thumb constraint extracted from human demonstration of grasping a ball. In Figure 6(a), without any constraint, the wrist can move around the circle, while in Figure 6(b), with the thumb constraint, the workspace of the wrist is constrained to rotate around only one contact point between the thumb and the object.

The feasible configuration space is also bounded by the desired grasp type. In addition, the grasp type also affects the number of variables to be optimized. The abduction/adduction angle θ_4 is under planning only for a sphere-type grasp, meaning that an abduction is needed for the task. In a sphere grasp planning, further simplification can be made to select one grasp from a set of candidate grasps, by dividing the search procedure into two stages. In the first stage, a search is run on a 2D space, θ_{33} and θ_3. The adduction/abduction angle θ_4 is searched for after θ_{33} and θ_3 are established, to reduce the number of resulting combinations of adduction/abduction angles and flexion/extension angles. Therefore, the computational complexity of the optimization procedure is reduced to $O(n^2)$.

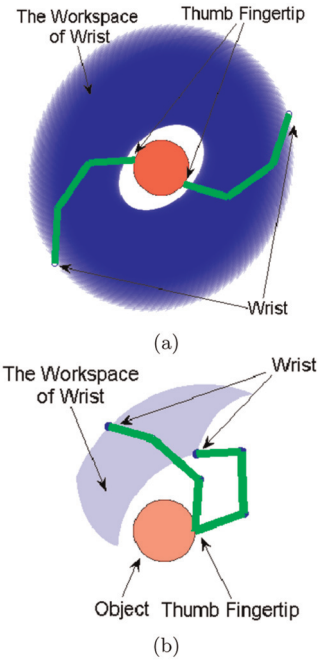

Fig. 6. Workspace of the Barrett hand (a) without constraint, and (b) with thumb constraint extracted from demonstration.

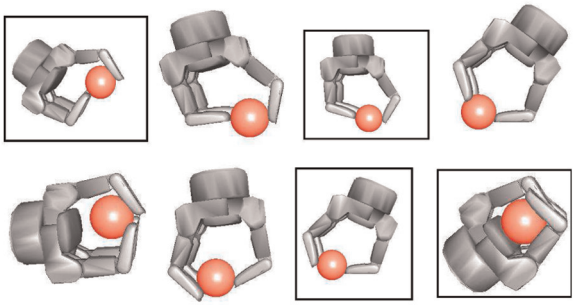

Fig. 7. An example of hand posture snapshots during a searching procedure. Postures bordered by a black box are grasps with an epsilon quality larger than 0.1.

An example of the searching procedure involving a Barrett hand grasping a sphere is presented in Figure 7, which shows snapshots of the current hand posture during optimization. Postures bordered by a black box are grasps with an epsilon quality larger than 0.1. During the execution, the contact point between the thumb and the object remains the same, while the pitch of the thumb changes.

4.1. Generalization to other robotic models

The proposed method can also be extended to other robotic models. Take the Shadow hand for instance, which is

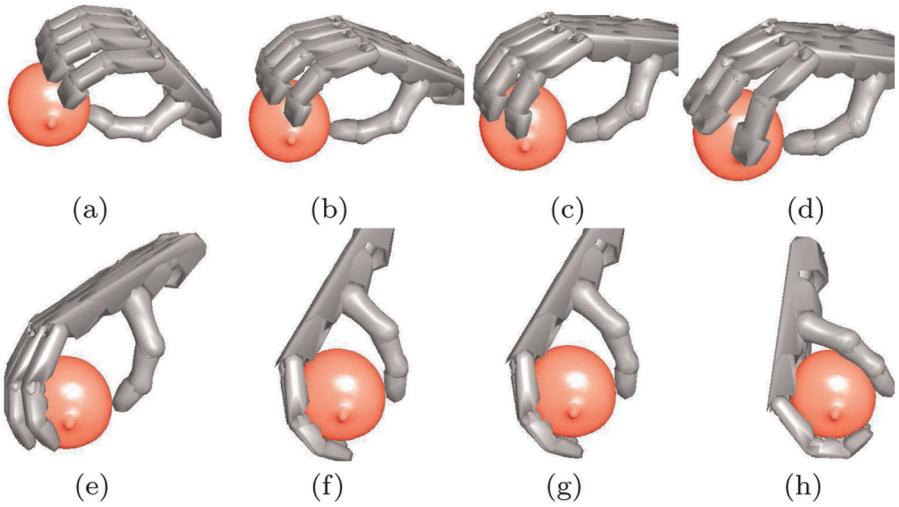

Fig. 8. A procedure of the Shadow hand searching for a power sphere grasp; (d) is a precision sphere grasp, which is rejected because it is not a desired grasp type; (h) is a desired power sphere grasp.

designed to closest approximate the human hand (Kochan, 2005). The objective function is the same as equation (4), $Q = f(p,\ w)$, where $p = [\theta_1,\ldots,\theta_D]^{\mathrm{T}}$ is a vector of finger joints, and D is the number of finger joints; $D = 22$ for a Shadow hand excluding two additional joints in the wrist. Similar to the Barrett hand, once the thumb position is extracted from demonstration, the wrist position and orientation w can be determined via forward kinematics by both the pitch of thumb relative to the object, and the thumb joint variables. The workspace of the wrist is highly constrained by the posture of the thumb. Therefore, the objective function becomes

$$Q = f(p, \gamma) \tag{12}$$

where γ is the thumb pitch relative to the object. The search space of the optimization depends on the DOFs of the hand joints p.

Further dimensionality reduction can be performed on hand DOFs using some existing approaches. The idea of dimensionality reduction on finger joints was proposed by Santello et al. (1998), who performed PCA on the human hand motion data and revealed that the first two eigengrasps (mainly flexion/extension and adduction/abduction) capture more than 80% variance of the grasp motions, implying a substantial simplification on hand postures. The idea of eigengrasp was applied by Ciocarlie and Allen (2009) in grasp planning, where the DOFs of hand and wrist are reduced to eight. The two dominant eigengrasps are sufficient for power grasps, where less dexterity is desired. In dexterous manipulation tasks, however, a different choice of simplified DOFs is needed for precision grasps.

Hand posture p can be described as a function g of the reduced DOFs e_i, written as

$$p = g(e_i), \quad i = 1, \ldots, d \tag{13}$$

where $d << D$ is the number of reduced DOFs. The function g and the value of d differ by grasp types. The wrist position can be determined by thumb posture, written as

$$p = h(e_i, \gamma) \tag{14}$$

Therefore, equation (4) can be simplified and generalized as

$$Q = f(e_i, \gamma) \tag{15}$$

Hence, the dimensionality of the searching space equals $d + 1$. If the number of DOFs of finger joints is reduced to two, then the searching space has three dimensions. An example of power sphere grasp planning is illustrated in Figure 8, searching through the subspace of relative pitch γ.

4.2. Generalization on thumb placement

Thumb placement can be obtained by observing human demonstration. Observing human demonstration put one thumb placement constraint on the grasp searching which assumes that the same thumb contact point is reachable by the robot. Alternatively, a set of thumb placements can be labeled directly on the object surface. Therefore, the candidate grasp can be computed from a set of given thumb placements on the object surface considering the kinematics limitations as well as the reachability properties.

The upper left of Figure 9 shows an example of a labeled area. The participants were asked to label colors on the object to indicate the contact area and direction of the thumb. The thumb can be placed only on the colored area, with different colors specifying different thumb directions relative to the principal axes of the object. Thumb placement in the green-colored area can be pointed only to the object's axis y, while thumb placement in the blue-colored area can be pointed only to the object's axis z. The

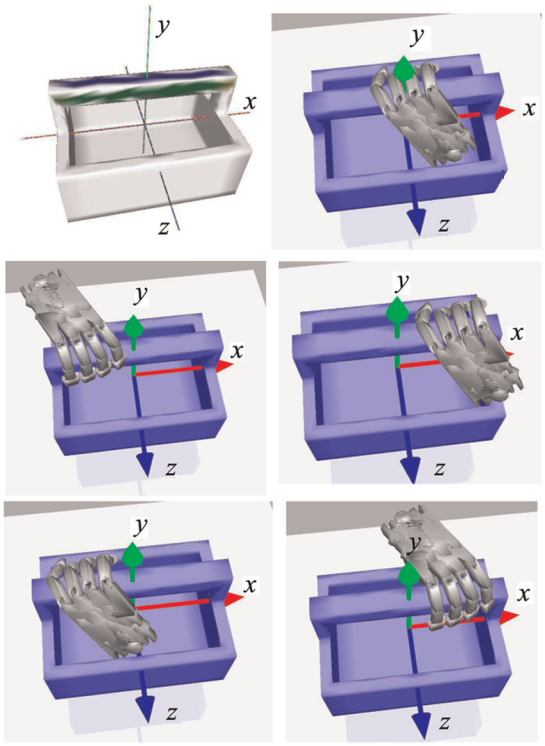

Fig. 9. Illustration of searching procedure constrained by thumb placement and direction. The colored area in the first figure is the area where the thumb is allowed to be placed. Thumb placement in the green-colored area can be pointed only to axis *y*, while thumb placement in blue-colored area can be pointed only to axis *z*.

following images of Figure 9 show snapshots of a searching procedure of a power grasp throughout the constraint area of thumb placement, where a power grasp is specified.

The number of grasps to be searched for depends on simulation settings, such as resolution of the object model, step size of the search space, and the physical robotic hand. Taking the tote tool in Figure 9 for example, for one single constraint of thumb placement, if the step size of searching is set to be five degrees in the configuration space, around 250 candidate grasps will be evaluated. The object model has 5666 faces in total, with 161 labeled thumb placements and directions on the handle. Thus, 40,250 candidate grasps would be evaluated overall with the thumb labels, whereas without the constraint, the hand can be put anywhere in any direction on the object, and the number of grasps will be much larger. Instead of exhaustive searching, of course, further improvement can be made for the optimization procedure.

5. Experiment

5.1. Evaluation on grasp type recognition

We measured the sequence of hand motions for grasp type extraction using a right-handed 5DT Data Glove 14 Ultra, with 14 fiber-optic-based bend sensors measuring the amount of bending, shown in Figure 10. It captures proximal interphalangeal (PIP) articulations and metacarpophalangeal (MP) joints for all the five fingers, and MP joints between adjacent fingers. The flexure resolution is 12-bit for each sensor, and the minimum dynamic range is 8-bit. The sensor does not measure real joint angles. Instead, it measures the proportion of bending of the measuring joint in its full range of motion. The bending values are scaled in-between 0 and 1, with 0 being fully open and 1 being fully closed. Hand motions from fully open to closed were sampled at a rate of 100 Hz.

In the experiment, 12 human grasp types were defined for the human hand, as illustrated in Figure 10. Eighteen everyday objects were tested (Figure 11). Each object is associated with some predefined grasp types. For example, a screwdriver is associated with small wrap grasp and adducted thumb grasp, and a dry-erase marker is associated with precision grasp and small wrap grasp. Four subjects participated in the experiment and were asked to grasp each of the objects using the designated grasp types. They were taught every grasp type by an expert. To demonstrate a grasp, they initially opened their hands, and the object was placed in front of their palms. Then, they closed their fingers to grasp the object as instructed. Each demonstration was performed for five trials.

For *k*NN recognition, we chose k to be 5. The dimensionality of motion data is reduced to three. To evaluate the recognition rate using grasp trajectories, we compared our results with the recognition rate in the approach using final grasp poses. The grasp poses were extracted from the grasp trajectories in the training dataset. Similar to the dimensionality reduction we applied to the grasp motion sequence, the dimensionality of the 14-DOF hand poses were also reduced to three using LDA. LDA (Fisher, 1936) is a popular linear dimensionality reduction approach commonly applied for recognition purposes that projects data points into subspaces, maximizing linear class separability and minimizing the within-class variance. To compare the results between our approach and the LDA approach, cross-validations were performed to assess the recognition rate for both known and unknown objects (new objects). For cross-validation of known objects, each motion trajectory of all 18 objects was left out of the training dataset for validation while the remaining trajectories were used for training. For cross-validation of unknown objects, all trajectories of each object were used for validation, while the trajectories of the remaining objects were used for training.

The results are reported in Table 1: for known objects, our approach is slightly better than the LDA approach, while for unknown objects, our approach has an 11% improvement over the LDA approach in the recognition rate. Detailed comparisons of the recognition rates of all 12 grasp types for unknown objects are presented in Figure 12. It can be observed that the proposed approach has higher recognition rates than the approach using static grasping poses for all grasp types.

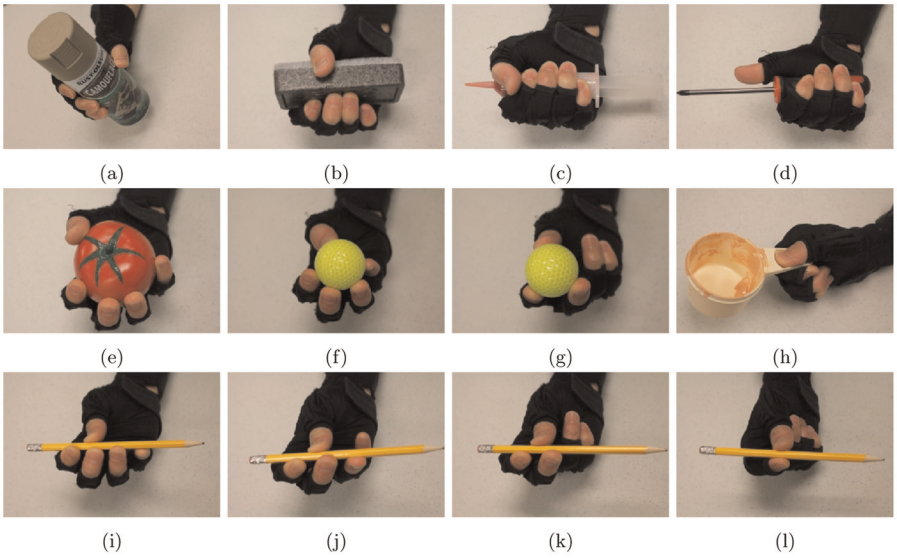

Fig. 10. Twelve human grasp types used for training. (a) Large wrap; (b) medium wrap; (c) small wrap; (d) adducted thumb; (e) power sphere; (f) precision sphere; (g) tripod; (h) lateral pinch; (i) four-finger-thumb precision; (j) three-finger-thumb precision; (k) two-finger-thumb precision; (l) one-finger-thumb precision.

Fig. 11. Daily grasping objects used in the experiment.

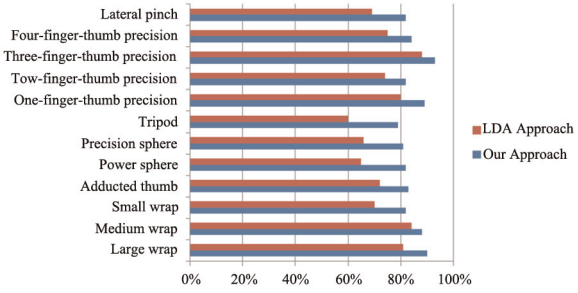

Fig. 12. Recognition rates of our approach and the LDA approach for unknown objects.

Table 1. Mean absolute percentage error between estimated grasp poses and the best grasp poses.

Testing Object	Our Approach	LDA Approach
Known Object	96%	94%
Unknown Object	85%	74%

In addition, we performed cross-validations on unknown users (new demonstrators). In each of the four validations, one of the four subjects was selected in order and the subject's grasp motion data was used for evaluation, and the remaining subjects' grasp motion data was used for training. Due to the limitation of the data glove, which has a large variation in measuring joint angles across users because of large geometry variances between human hands, the recognition rate dropped to 61%. This is still comparable with other works (Ekvall and Kragic, 2005; Aleotti and Caselli, 2006; Heumer et al., 2007), even though our experiments were tested with more grasp types. Our study (Dai et al., 2013) found that the differences between several grasp types are not significant based on the hand poses or motion when considering the difference between human hands.

Figure 13 illustrates three irregular grasps of a box, a pair of pliers, and a gun. The first column is the human demonstration. Columns 2 and 3 compare 3D representation of 14D demonstrated motion trajectories and poses. The trajectory marked by black stars is the testing grasp.

In Figure 13(a), the participant demonstrated a large-wrap-like grasp of a box, where the little finger closed more than the other fingers. Figure 13(b) shows that the trajectory of the demonstrated grasp was similar to the trajectories belonging to the large wrap grasp in the training dataset. The five nearest neighbors of this demonstration were all trajectories in the large wrap grasp type. Figure 13(c) shows that the nearest neighbors of the demonstrated poses were the four-finger precision and tripod grasp types.

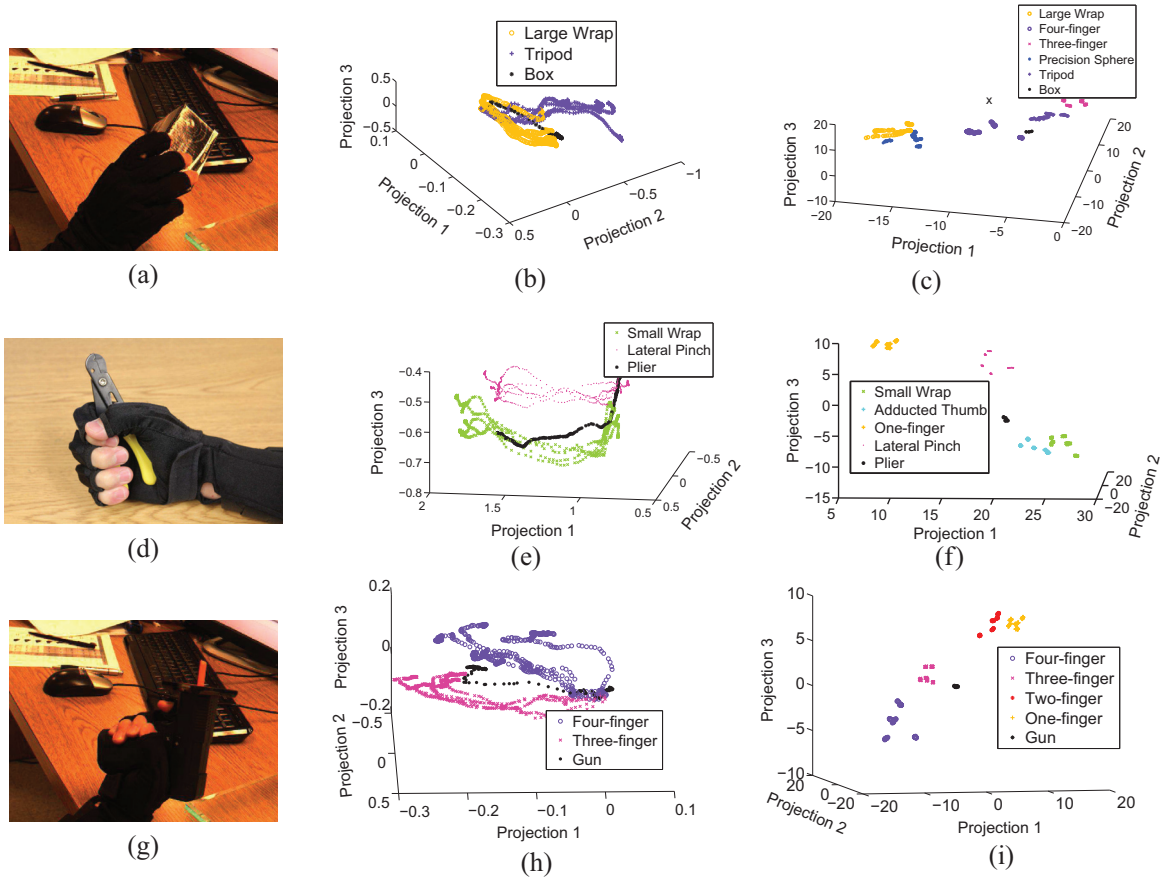

Fig 13. Three grasp examples: Column 1, human demonstration; Column 2, 3D representation of 14D hand motion trajectories using LPP; Column 3, 3D representation of 14D static hand pose using LDA.

The second row illustrates a grasp of a pair of pliers. The nearest trajectories belonged to small wrap (Figure 13(e)), and the nearest poses belonged to small wrap and lateral pinch (Figure 13(f)).

The third row is the example of grasping a gun. The user employed a medium-wrap-like grasp, but the index finger was put on the trigger. The trajectory of grasping a gun was between four-finger precision and three-finger precision (Figure 13(g)), and the nearest neighbor of the grasp pose is three-finger precision (Figure 13(h)).

Fewer grasp types can be defined for the robotic hand when mapping from the human, because robotic hands usually have fewer DOFs and therefore less dexterity. Fewer grasp types would also improve recognition. Taking the Barrett hand model for example, we defined only five grasp types, much fewer than the human hand: power grasp, power sphere, precision grasp, precision sphere, and lateral pinch. Some grasp types can be grouped into one. For example, four-finger-thumb precision, three-finger-thumb precision and two-finger-thumb precision grasps can be grouped together as a precision grasp for a robotic model when the two fingers opposite the thumb are adducted. Table 2 shows the corresponding grasp types between a human and a Barrett hand.

The five grasp types of the Barrett hand decide how the search space of the optimization procedure can be reduced:

Table 2. The dictionary of the corresponding grasp types between the human and the robotic hand.

Human Grasp Types	Robot Grasp Types
Large Wrap	Power
Medium Wrap	
Small Wrap	
Adducted Thumb	
Power Sphere	Power Sphere
Precision Sphere	
Tripod	Precision Sphere
Four-finger-thumb Precision	Precision
Three-finger-thumb Precision	
Two-finger-thumb Precision	
One-finger-thumb Precision	
Lateral Pinch	Lateral Pinch

whether the grasp is a power grasp or not determines whether the object should be in contact with the palm; and whether the grasp is a sphere grasp or not determines whether the search subspace of the spread angle can be rejected. If it is not a sphere grasp, the dimensionality of the search space can be reduced to two by commanding the Barrett hand to adduct completely. Determination of the sphere type is necessary because, in the experiment, we found that a sphere grasp with a larger spread angle usually

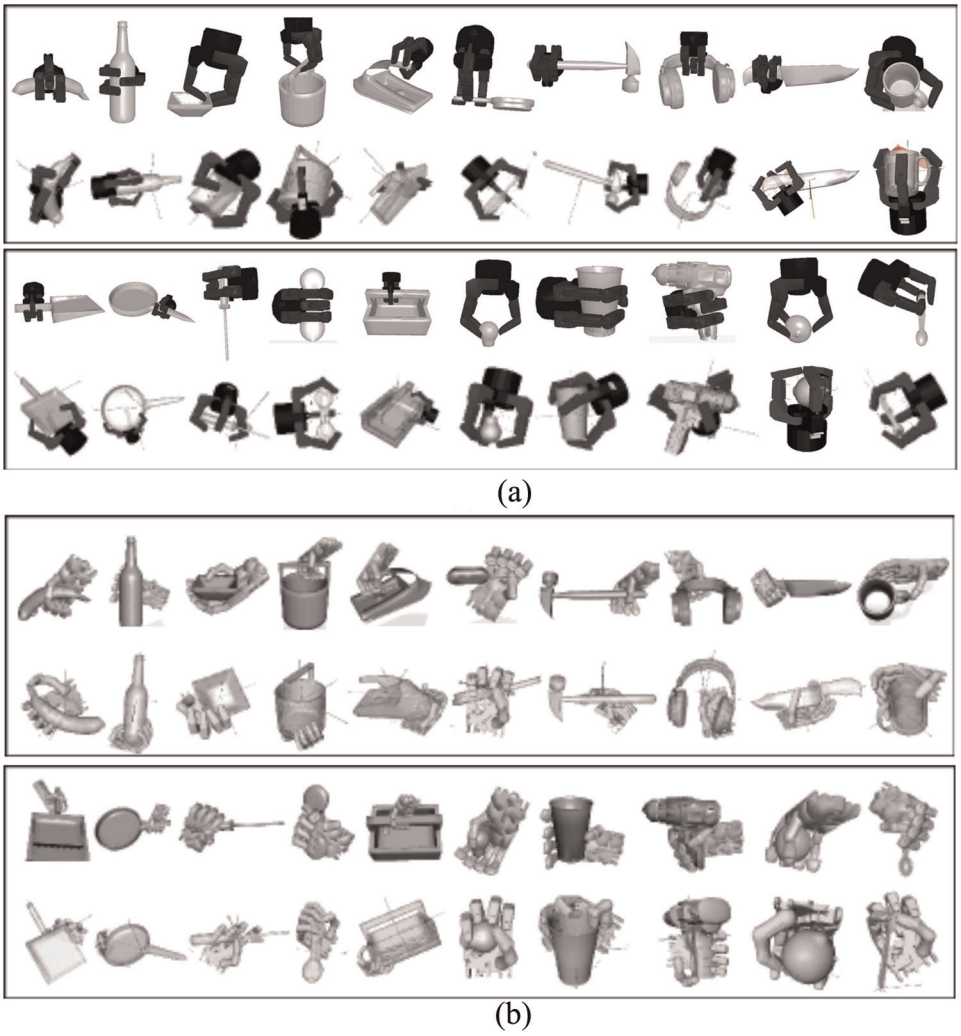

Fig. 14. Comparison between the top-ranking grasps selected by our approach and GraspIt! for (a) the Barrett hand model, and (b) the Shadow hand model.

has a higher-quality measure than a non-sphere grasp type without a spread angle, while Balasubramanian et al. (2010) pointed out that humans tend to use low spread pinch, which leads to lower force-closure quality but a higher success rate.

For other robotic hand models, of course, the grasp types can be defined dependent on the level to which the robotic hand is a simplification of the human hand. For example, the same grasp types can be defined for the Shadow hand as for the human hand, as it has similar dexterity to the human hand.

5.2. Evaluation on resulting simulated grasps

In the experiment, grasp type, thumb position and orientation were obtained from the human demonstration. The thumb position relative to the object of the demonstration was captured by an OptiTrack Mocap system, with reflecting markers on the thumb and the object. The joint angles were captured by the 5DT data glove.

In simulation, we set the friction coefficient μ to be 0.9. The friction cone is approximated by an eight-sided pyramid. Thus, each contact point has eight unit wrench vectors. The computation is expensive for a convex hull, so we set the step size to be five degrees for all the angles. The grasp quality measure for the optimization was the commonly used epsilon quality, defined as the radius of the largest wrench ball that is enclosed by the grasp wrench space (Ferrari and Canny, 1992). It provides a way to quantify the force-closure property, which is the necessary condition for a stable grasp. Of course, other grasp quality measures can also be used, such as the one that considers task wrench space in the measure to emphasize the ability of the grasp to resist large force disturbance in some direction (Sun, 2011; Lin and Sun, 2013b).

To evaluate the proposed approach, simulation results of the Barrett hand model and the Shadow hand model were evaluated to compare our own simulator with the well-known simulator GraspIt!. Twenty daily objects and manipulative tools as listed in Table 3 were tested in the experiments, which comprise basic shapes such as cuboids, spheres and

Table 3. Twenty objects evaluated in simulation.

No.	Object Name	No.	Object Name
1	Banana	11	Dust pan
2	Beer bottle	12	Frying pan
3	Square bowl	13	Screwdriver
4	Bucket	14	Telephone handset
5	Clothes iron	15	Basket
6	Headphones	16	Light bulb
7	Hair brush	17	Cup
8	Hammer	18	Power drill
9	Kitchen Knife	19	Onion
10	Mug	20	Spoon

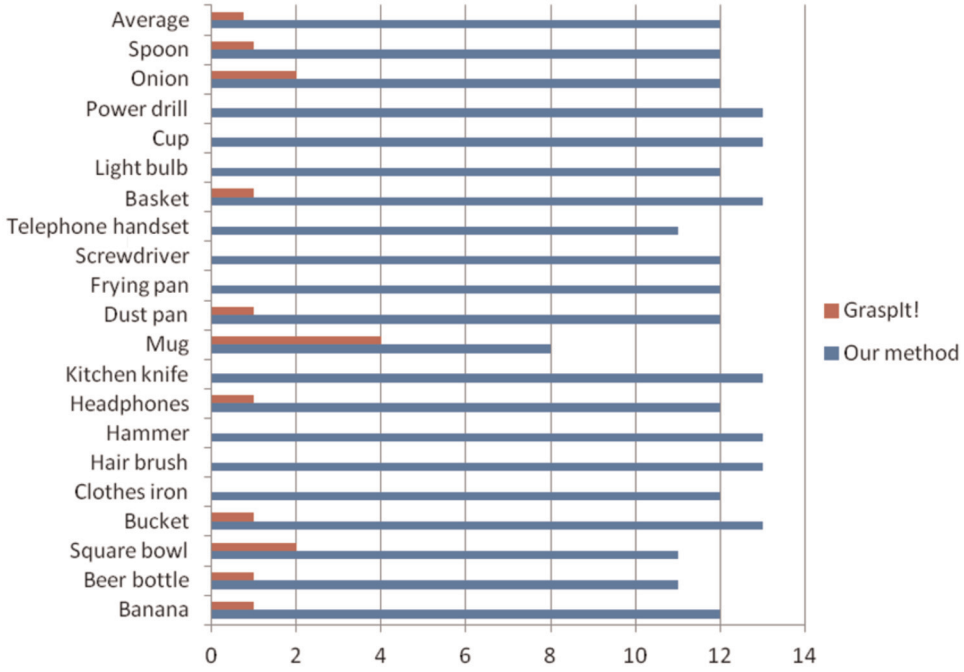

Fig. 15. The choice of 13 human participants in their preferred grasps for the Barrett hand model, concerning the functionality and shape of the target object. Multiple choices or none can be made. On average, 92.31% considered the grasps selected by our approach as close to their intuitive ones, compared with 5.77% of GraspIt!.

cones. These basic shapes form the majority of daily objects and manipulative tools. The top-ranking grasp of every object, as compared in Figure 14 for the Barrett hand and Shadow hand, were selected by our approach and Graspit!.

To quantitatively evaluate each grasp in relation to the functionality and shape of the target object, we introduced a human survey to examine each grasp, as we believe that humans are experts in grasping. Therefore, we relied on human participants to use their intuition and experience in choosing a grasp suitable for an object to evaluate the simulated grasps. Thirteen people participated and were asked to choose the grasps they would like the robot to use, considering the functionality and shape of the objects. The resulting grasps from both simulators were randomly ordered, and the color of the object models and hand models were set the same to minimize bias and eliminate any clue from the appearances of the two simulators. The participants were instructed to select all the good grasps from all the grasping results generated by both approaches.

Figures 15 and 16 report the grasp choices by 13 human participants for the Barrett hand model and Shadow hand model respectively. On average, for the Barrett hand model, 92.31% selected the grasps resulting from our approach, compared with 5.77% of GraspIt!, while for the Shadow hand model, 85.77% selected the grasps resulting from our approach, compared with 10.38% of GraspIt!. For the majority of the grasps, more people thought the grasps resulting from our approach are the ones they would prefer the robot to use. The exceptions are the banana, light bulb and mug in Shadow hand evaluation. One reason is the static object assumption in most of the existing simulators (Kim et al., 2013). In the real world, the object may be

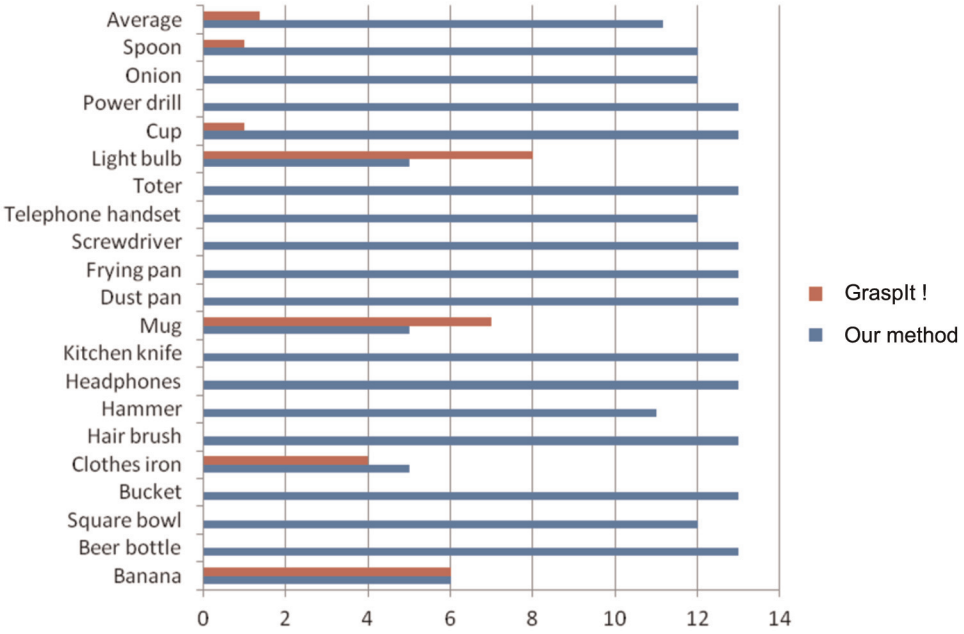

Fig. 16. The choice of 13 human participants in their preferred grasps for the Shadow hand model, concerning the functionality and shape of the target object. Multiple choices or none can be made. On average, 85.77% selected the grasps resulting from our approach, compared with 10.38% of GraspIt!.

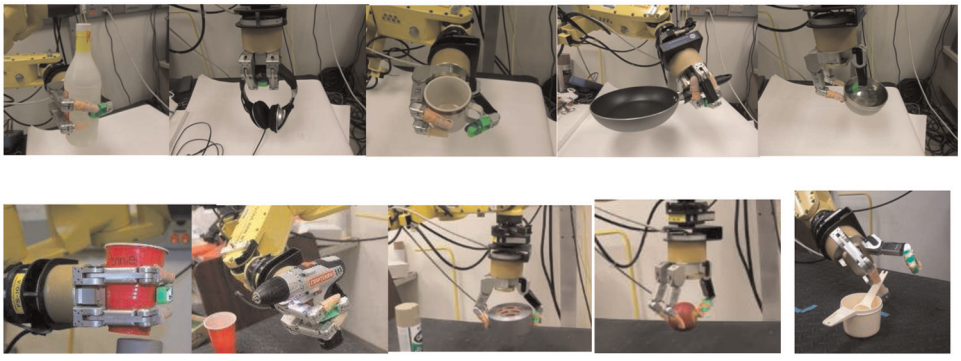

Fig. 17. Experiment on real robotic platform.

moved by the fingers after contact, but this property is not implemented in simulation. The grasp planner had trouble finding a grasp for the mug that was like that of humans, who tend to wrap their fingers around the handle. Although the resulting grasp by the planner has a high force-closure property, it was not very robust in the real world.

Based on the observations from the simulation and the human survey, without integrating grasp type and the thumb placement into the planning, GraspIt! tends to select an encompassing grasp for each object, while with the integration of the extracted strategy from humans, the resulting grasps are more close to human-style grasps.

5.3. Experiment on real robotic platform

We also tested the proposed approach with a real Barrett hand equipped on a 6-DOF FANUC LR MATE 200iC robotic arm. Ten daily objects were evaluated and the grasp success rates were reported, shown in Figure 17. Each grasp was executed for 10 trials. The object was placed at the same predefined known position and orientation in the robot workspace every time, without any obstacles between the robot and the target object. The accurate geometric model of the object was also obtained. The robot first moved to the target object and grasped the object in a resulting pose from planning, and then the robot lifted the target object. The position error was around 1 cm on average. We judge a grasp to be successful if the robot can hold the object stably. A grasp is regarded as a failure if the object is dropped or slides out of the hand.

As reported in Table 4, we achieved a success rate of 79% for the 10 objects. For most of the time, our approach was able to lift the object without dropping it. Overall, the power grasp could achieve a higher success rate than the precision

Table 4. Success rate in real experiment.

Object Name	Grasp Success Rate
Beer bottle	100%
Headphones	100%
Mug	80%
Frying pan	90%
Bowl	70%
Cup	100%
Power drill	80%
Ducted tape	70%
Onion	60%
Spoon	40%
Overall	79%

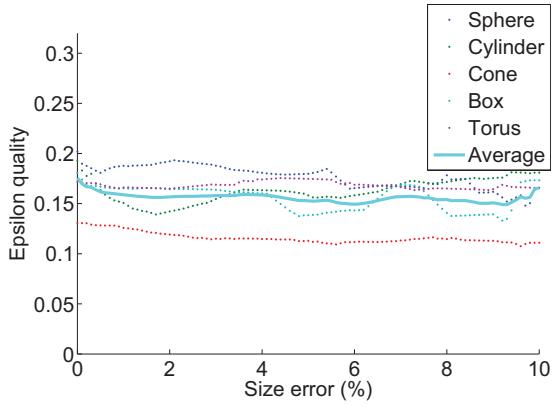

Fig. 18. The epsilon quality measures at different object size errors.

grasp (the bowl, tape and onion). The failure grasps were mostly caused by position errors. For example, the pinch grasp for the spoon has the lowest success rate of 40% due to a considerable position error for relatively small objects.

Although the purpose of the proposed approach is to find the grasps by incorporating human strategies, and the search space was confined by the grasp types and thumb placements, the results are still comparable with the success rate of 77% for GraspIt! reported in Balasubramanian et al. (2010). In addition, the grasps tested in their works were all power grasps, while our experiment included precision grasps, which are usually more sensitive to position errors.

5.4. Studies on the robustness to uncertainty

It is a common problem that uncertainty exists in the perception of human demonstrations, as well as the pose estimation of the object. Noisy sensors also cause errors in perceptions of the shape and pose of an object. In our method, it is important to study how accurate the perception of human demonstrations and the object needs to be so that the grasp is not broken by uncertainty. We conducted experiments in simulation to examine how robust the resulting grasps of the proposed method are in resisting small perception errors on object geometry and the thumb

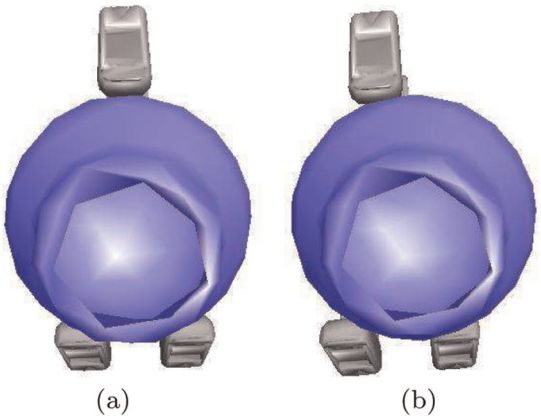

Fig. 19. A visible thumb position error of 20 mm in simulation. (a) Original thumb position; (b) thumb position with a 20 mm error.

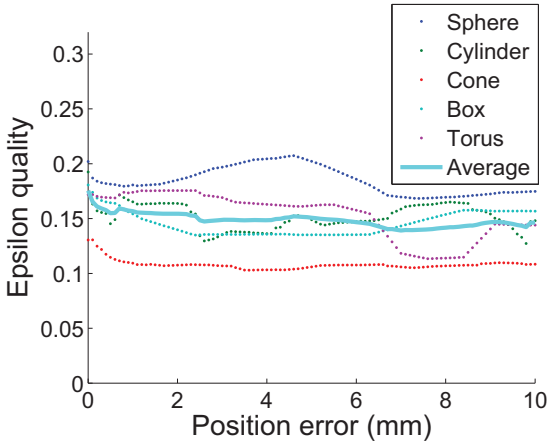

Fig. 20. The epsilon quality measures at different thumb position errors.

position relative to the target object. Five objects, including a sphere, a box, a cylinder, a torus and a cone, were tested in the experiment. We only tested precision grasp because perception error is of higher concern for precision grasp than power grasp.

The introduction of object geometry errors can be implemented by perturbing the object size. Because the result of every size error was the same for every execution in the simulation, each size error was executed once. Figure 18 shows the quality measures of the five objects models with slightly changing sizes from 0% to 10%. Since a grasp is considered to be a stable grasp when the epsilon quality is 0.1 or greater, although there was some error in the grasp qualities, the stability of the grasp was not changed.

Thumb position relative to an object is easily shifted in simulation, thereby making it easy to simulate position errors. For example, in Figure 19, the thumb is shifted slightly to the left of the real position, with a visible position error of 20 mm. Figure 20 illustrates how the

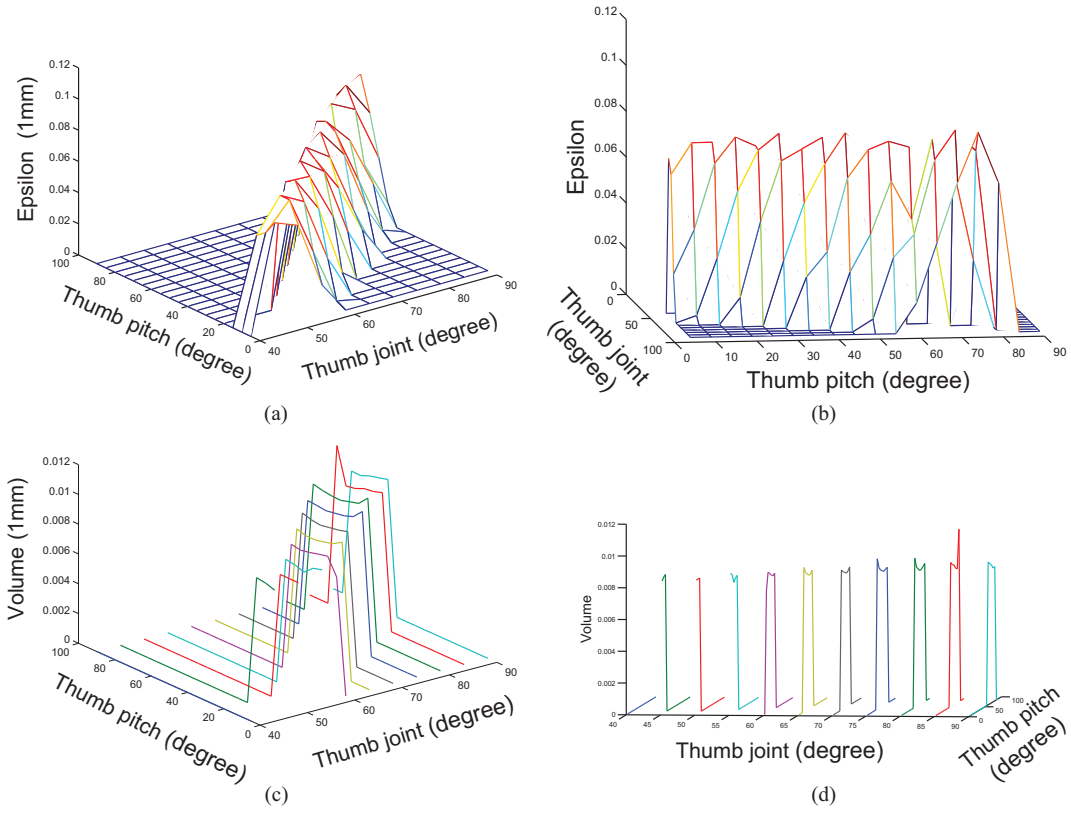

Fig. 21. The grasp quality measures of a precision grasp vs thumb pitch relative to the object and thumb joint angles. (a) and (b) Epsilon grasp quality from two view angles; (c) and (d) volume grasp quality from two view angles.

epsilon quality is changed at different thumb position errors from 0 mm to 10 mm. According to the results, the resulting grasp presented some robustness to small position errors.

6. Discussions

Precision grasps are vital in dexterous manipulation. Generally, people would first apply a precision grasp with only the fingertips in contact with an object when they pick it up. Then, they perform in-hand manipulation to get a better closure around the object for the subsequent manipulation.

Figure 21 shows the quality measure of a precision grasp optimization involving grasping an ashtray with respect to relative thumb pitch and thumb flexion angle. The ridge shape of the quality measure implies that the planning results in more than one optimal precision grasp quality, indicating a set of compositions of thumb pitch and thumb flexion angle. The postures of different hand compositions are shown in Figure 22. The resulting grasps indicate a rolling manipulation, where the contact points remains the same but the hand postures vary, demonstrating that manipulation flexibility of the precision grasp resulted from the proposed method.

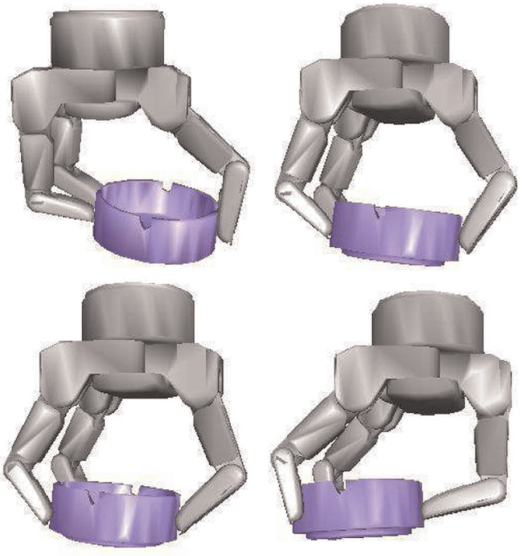

Fig. 22. Four different hand postures along the ridge of the quality measure surface.

7. Conclusions

In this paper, we propose grasp type and thumb placement, which commonly exist in almost all grasps, as general

grasp abstractions from human demonstration. They also provide partial constraints of hand postures and wrist positions and orientations, but leave enough room and flexibility to accommodate the differences between a human hand and a robotic hand. Due to geometry differences between human hands, some grasp types cannot be reliably recognized for a new human demonstrator. Therefore, for a new demonstrator, a user-specific calibration procedure is recommended.

The presented approach was tested in simulation with a Barrett hand and a Shadow hand for 20 objects and the generated grasps for the objects were evaluated by 13 human participants using their intuition and experience. Based on the results, we concluded that without integrating grasp type or thumb placement into the planning, GraspIt! tends to select an encompassing grasp for each object, while our approach with the integration of the extracted strategy from humans generated grasps more close to human-style grasps. We also demonstrated in the experiment how robust the approach was to perception uncertainties. The presented approach was also evaluated with a real robotic system, to compare with the non-task-specific automatic grasp planning. The proposed method can be generalized to other robotic models by combining it with the dimensionality reduction of a hand model. Further studies will be performed in the future.

However, grasp optimization by force-closure property with the constraints of grasp type and thumb placement does not always find human intent grasps, like the resulting grasp for a mug shown in Figure 14 (the last grasp in row 1). Although the thumb is specified to be placed on the handle, the other fingers do not insert into the handle, but wrap around the mug body instead. Therefore, depending on applications and task requirements, additional grasp characteristics may be needed. For example, for grasping a cup to pour water, a hand should not block the open surface of the cup; a finger should be on the trigger when using a power drill or firing a weapon.

In the current research, we did not consider grasp planning for novel objects, which has been exploited by other researchers. Example works include Saxena et al. (2008), Li et al. (2007), Papazov et al. (2012) and Kootstra et al. (2012). The proposed approach can be easily combined with other algorithms adaptive to novel objects. In the future, potential research can be conducted in this direction. Grasp planning can be performed by matching a similar shape in the database of objects with a labeled thumb contact point and task-specific grasp type.

Funding

This work was supported, in part, by the University of South Florida Research & Innovation Internal Awards Program under Grant No. 0074381.

References

Aleotti J and Caselli S (2006) Grasp recognition in virtual reality for robot pregrasp planning by demonstration. In: *IEEE international conference on robotics and automation*, pp. 2801–2806.

Balasubramanian R, Ling X, Brook PD, et al. (2010) Human-guided grasp measures improve grasp robustness on physical robot. In: *International conference on robotics and automation*, pp. 2294–2301.

Belkin M and Niyogi P (2001) Laplacian eigenmaps and spectral techniques for embedding and clustering. In: *NIPS*, pp. 585–591.

Ben Amor H, Kroemer O, Hillenbrand U, et al. (2012) Generalization of human grasping for multi-fingered robot hands. In: *IEEE/RSJ international conference on intelligent robots and systems*, pp. 2043–2050.

Butterfass J, Grebenstein M, Liu H, et al. (2001) DLR-Hand II: Next generation of a dextrous robot hand. In: *IEEE international conference on robotics and automation*, pp. 109–114.

Ciocarlie MT and Allen PK (2009) Hand posture subspaces for dexterous robotic grasping. *The International Journal of Robotics Research* 28(7): 851–867.

Cutkosky MR (1989) On grasp choice, grasp models, and the design of hands for manufacturing tasks. *IEEE Transactions on Robotics and Automation* 5(3): 269–279.

Dai W, Sun Y and Qian X (2013) Functional analysis of grasping motion. In: *IEEE/RSJ international conference on intelligent robots and systems*.

Ekvall S and Kragic D (2005) Grasp recognition for programming by demonstration. In: *IEEE international conference on robotics and automation*, pp. 748–753.

El-Khoury S and Sahbani A (2010) A new strategy combining empirical and analytical approaches for grasping unknown 3D objects. *Robotics and Autonomous Systems* 58(5): 497–507.

Ferrari C and Canny J (1992) Planning optimal grasps. In: *IEEE international conference on robotics and automation*, pp. 2290–2295.

Fischer M, van der Smagt P and Hirzinger G (1998) Learning techniques in a dataglove based telemanipulation system for the DLR hand. In: *IEEE international conference on robotics and automation*, pp. 1603–1608.

Fisher RA (1936) The use of multiple measurements in taxonomic problems. *Annals of Eugenics* 7(2): 179–188.

Gioioso G, Salvietti G, Malvezzi M, et al. (2011) Mapping synergies from human to robotic hands with dissimilar kinematics: An object based approach. In: *IEEE international conference on robotics and automation*.

Heumer G, Amor HB, Weber M, et al. (2007) Grasp recognition with uncalibrated data gloves – A comparison of classification methods. In: *IEEE virtual reality conference*, pp. 19–26.

He X and Niyogi P (2003) Locality preserving projections. In: *NIPS*.

Hotelling H (1933) Analysis of a complex of statistical variables into principal components. *Journal of Educational Psychology* 24(6): 417.

Hsiao K and Lozano-Perez T (2006) Imitation learning of whole-body grasps. In: *IEEE/RSJ international conference on intelligent robots and systems*, pp. 5657–5662.

Hueser M, Baier T and Zhang J (2006) Learning of demonstrated grasping skills by stereoscopic tracking of human head configuration. In: *IEEE international conference on robotics and automation*, pp. 2795–2800.

Jacobsen SC, Wood JE, Knutti DF, et al. (1984) The Utah/MIT dextrous hand: Work in progress. *The International Journal of Robotics Research* 3(4): 21–50.

Kang SB and Ikeuchi K (1997) Toward automatic robot instruction from perception-mapping human grasps to manipulator grasps. *IEEE Transactions on Robotics and Automation* 13(1): 81–95.

Kim J (2007) *Example-based grasp adaptation*. PhD Thesis, Massachusetts Institute of Technology, MA.

Kim J, Iwamoto K, Kuffner J, et al. (2013) Physically based grasp quality evaluation under pose uncertainty. *IEEE Transactions on Robotics* 29(6): 1424–1439.

Kochan A (2005) Shadow delivers first hand. *Industrial Robot: An International Journal* 32(1): 15–16.

Kootstra G, Popović M, Jørgensen JA, et al. (2012) Enabling grasping of unknown objects through a synergistic use of edge and surface information. *The International Journal of Robotics Research* 31(10): 1190–1213.

Le QV, Kamm D, Kara AF, et al. (2010) Learning to grasp objects with multiple contact points. In: *IEEE international conference on robotics and automation*, pp. 5062–5069.

Lin Y and Sun Y (2013a) Grasp mapping using locality preserving projections and kNN regression. In: *International conference on robotics and automation*.

Lin Y and Sun Y (2013b) Task-oriented grasp planning based on disturbance distribution. In: *International symposium on robotics research (ISRR)*.

Lin Y, Ren S, Clevenger M, et al. (2012) Learning grasping force from demonstration. In: *IEEE international conference on robotics and automation*, pp. 1526–1531.

Liu G, Xu J, Wang X, et al. (2004) On quality functions for grasp synthesis, fixture planning, and coordinated manipulation. *IEEE Transactions on Automation Science and Engineering* 1(2): 146–162.

Li Y, Fu JL and Pollard N (2007) Data-driven grasp synthesis using shape matching and task-based pruning. *IEEE Transactions on Visualization and Computer Graphics* 13(4): 732–747.

Lovchik CS and Diftler MA (1999) The Robonaut hand: A dexterous robot hand for space. In: *IEEE international conference on robotics and automation*, pp. 907–912.

Marzke MW and Marzke RF (2000) Evolution of the human hand: Approaches to acquiring, analysing and interpreting the anatomical evidence. *Journal of Anatomy* 197(1): 121–140.

Napier JR (1960) Studies of the hands of living primates. In: *Proceedings of the Zoological Society of London*, pp. 647–657.

Napier JR (1965) Evolution of the human hand. In: *Proceedings of the Royal Institution of Great Britain*, pp. 544–557.

Nguyen VD (1988) Constructing force-closure grasps. *The International Journal of Robotics Research* 7(3): 3–16.

Oztop E and Arbib MA (2002) Schema design and implementation of the grasp-related mirror neuron system. *Biological Cybernetics* 87(2): 116–140.

Papazov C, Haddadin S, Parusel S, et al. (2012) Rigid 3D geometry matching for grasping of known objects in cluttered scenes. *The International Journal of Robotics Research* 31(4): 538–553.

Peer A, Einenkel S and Buss M (2008) Multi-fingered telemanipulation-mapping of a human hand to a three finger gripper. In: *The 17th IEEE international symposium on robot and human interactive communication*, pp. 465–470.

Pollard NS (2004) Closure and quality equivalence for efficient synthesis of grasps from examples. *The International Journal of Robotics Research* 23(6): 595–613.

Ponce J and Faverjon B (1995) On computing three-finger force-closure grasps of polygonal objects. *IEEE Transactions on Robotics and Automation* 11(6): 868–881.

Roa MA and Suárez R (2009) Finding locally optimum force-closure grasps. *Robotics and Computer-Integrated Manufacturing* 25(3): 536–544.

Romero J, Kjellstrom H and Kragic D (2009) Modeling and evaluation of human-to-robot mapping of grasps. In: *International conference on advanced robotics*, pp. 1–6.

Rosales C, Ros L, Porta JM, et al. (2011) Synthesizing grasp configurations with specified contact regions. *The International Journal of Robotics Research* 30(4): 431–443.

Roweis ST and Saul LK (2000) Nonlinear dimensionality reduction by locally linear embedding. *Science* 290(5500): 2323–2326.

Sahbani A, El-Khoury S and Bidaud P (2012) An overview of 3D object grasp synthesis algorithms. *Robotics and Autonomous Systems* 60(3): 326–336.

Santello M, Flanders M and Soechting JF (1998) Postural hand synergies for tool use. *The Journal of Neuroscience* 18(23): 10,105–10,115.

Saxena A, Driemeyer J and Ng AY (2008) Robotic grasping of novel objects using vision. *The International Journal of Robotics Research* 27(2): 157–173.

Sun Y (2011) Fingertip force and contact position and orientation sensor. In: *2011 IEEE international conference on robotics and automation (ICRA)*, pp. 1114–1119.

Susman RL (1998) Hand function and tool behavior in early hominids. *Journal of Human Evolution* 35(1): 23–46.

Tegin J, Ekvall S, Kragic D, et al. (2009) Demonstration-based learning and control for automatic grasping. *Intelligent Service Robotics* 2(1): 23–30.

Tenenbaum JB (1998) Mapping a manifold of perceptual observations. *Advances in Neural Information Processing Systems* 10: 682–688.

Young RW (2003) Evolution of the human hand: The role of throwing and clubbing. *Journal of Anatomy* 202(1): 165–174.

Zhu X and Wang J (2003) Synthesis of force-closure grasps on 3-D objects based on the *Q* distance. *IEEE Transactions on Robotics and Automation* 19(4): 669–679.

Zöllner R, Pardowitz M, Knoop S, et al. (2005) Towards cognitive robots: Building hierarchical task representations of manipulations from human demonstration. In: *IEEE international conference on robotics and automation*, pp. 1535–1540.